AUTHOR QUERIES – Chapter 5

CHAPTER 5

Figure 5.16 is not mentioned in the text. Please insert mention.

References

Ref. 22 E. Paci, *Biochim..Biophys. Acta* **2002**, 1595, 185–200 - is not mentioned? Please insert.

Ref. 55. H. Lesch, J. Schlichter, J. Friedrich, J.M. Vanderkooi, *Biophys. J.* 2004, accepted - published yet?

5
Pressure–Temperature Phase Diagrams of Proteins

Wolfgang Doster and Josef Friedrich

5.1
Introduction

One of the most peculiar features of proteins is their marginal stability within a narrow range of thermodynamic conditions. Biologically active structures can be disrupted by increasing or decreasing the temperature, the pressure, the pH or by adding denaturants. By disrupting a structure one can study its architecture and energetics. In this article we focus on the thermodynamic aspects of temperature and pressure denaturation. A variation of temperature inevitably leads to a simultaneous change of entropy and volume through thermal expansion. The advantage of using pressure as a thermodynamic variable is that volume-dependent effects can be isolated from temperature-dependent effects. Just as the increase in temperature drives the system in equilibrium towards states of higher entropy, a pressure increase will bias the ensemble of accessible states towards those with a smaller volume. This is the meaning of le Chatelier's principle. Thus, if the protein has the lower volume in its denatured form, the native structure will become unstable above a critical pressure. Similarly the opposite effect, stabilization of the native state by pressure, is sometimes associated with heat denaturation.

Packing defects in the water-excluding native state, reorganization of the solvent near exposed nonpolar side chains, and electrostriction by newly formed charges act as volume reservoirs which can lower the volume in the unfolded state. While dissociation of oligomeric proteins into subunits occurs at low pressures, i.e., below 200 MPa [1], pressures above 300 MPa are required to denature monomeric proteins. A number of useful review articles on this subject have been published recently (see, for example, Ref. [2]).

The isothermal compressibility of water (0.56/GPa) is quite small. At 11 000 m below sea level and pressures near 100 MPa, the density of water is only 5% higher than at ambient pressure. On the other hand, the density at the freezing transition changes by 9%. Moreover, proteins are 5–10 times less compressible than water. As a result, pressure-induced volume changes in proteins are quite small, typically 0.5% of the total volume at the unfolding transition. For monomeric proteins the difference corresponds approximately to the volume of five water molecules

Protein Folding Handbook. Part I. Edited by J. Buchner and T. Kiefhaber

ISBN: 3-527-30784-2

(5×18 mL mol^{-1}). Thus, minor volume changes often induce large structural rearrangements, where essentially incompressible matter is displaced. Therefore pressure can be a powerful structural gear. On the other hand, the microscopic interpretation of protein volume changes is still one of the difficult and unresolved questions of the field [3, 4].

Part of the problem arises from the fact that the denatured state itself is not very well defined [5]. It is generally assumed that thermal denaturing leads to a random coil state. As to pressure-induced denaturation and cold denaturation, there are indications that the denatured state is still compact and resembles the molten globule state [5–7]. How such a situation can be reconciled with the simple thermodynamic description of protein stability based on a two-state model has to be investigated in each case.

Below we present a thermodynamic frame for describing and interpreting protein stability phase diagrams. The main features are illustrated using our own results obtained with various optical techniques as well as with neutron scattering.

5.2 Basic Aspects of Phase Diagrams of Proteins and Early Experiments

The most striking thermodynamic properties of proteins are related to the hydrophobic effect. These are

- the large and positive heat capacity increment upon unfolding [8–10] and
- the phenomenon of cold denaturation.

The latter was first predicted by Brandts [11, 12] based on studies of heat denaturation on ribonuclease. The transition temperatures for cold denaturation are usually below the freezing point of most aqueous solutions at ambient pressure. However, under high pressure, water remains liquid down to much lower temperatures (-18 °C at 200 MPa, Figure 5.1).

Thus cold denaturation can be studied conveniently at elevated pressures under mild denaturing conditions, without the need to add denaturants.

The phase diagram of water (Figure 5.1) illustrates the relevance of the pressure–temperature plane for locating states of structural stability and for classifying their thermodynamic properties.

The slope of the phase boundary of liquid water and ice I is negative: increase in pressure extends the stability range of the liquid phase. The slope of the phase boundary is given by the ratio of the negative entropy change and the increase in specific volume at the freezing transition (Eq. (3)). The expansion ($+9\%$) causes substantial damage when biological material is frozen. In contrast, the slope of the liquid to ice III boundary is large and positive, since the corresponding volume change is small and negative. The application of high pressure to the liquid and then cooling into ice III minimizes the damage by volume changes (-3%) at the freezing transition.

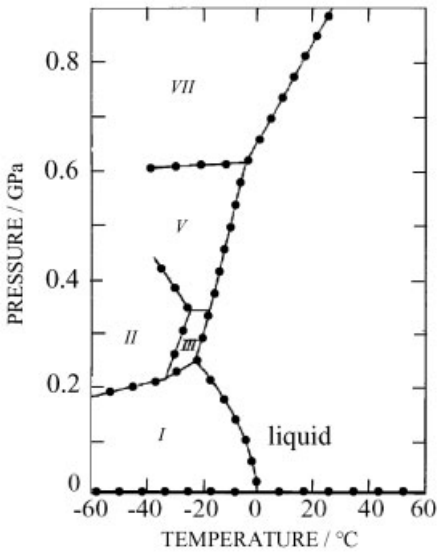

Fig. 5.1. The phase diagram of water: For the boundary from the liquid to hexagonal ice (I) one has $dP/dT = \Delta S/\Delta V < 0$, unlike for the technically relevant modifications, II and III where the volume discontinuity is small.

Proteins, consisting of a few thousand atoms, are mesoscopic objects. Experience and theoretical analysis shows [13] that they can be labeled by well-defined thermodynamic averages, such as the specific heat capacity, the compressibility, and the thermal expansion. The structural reorganization may then be regarded as a change of the macroscopic state of the system. Such changes occur in a highly cooperative manner. Since the native and denatured states of proteins differ not only in heat capacity but also in volume and entropy, the transition between the two states must involve a discontinuity in the first derivatives of the thermodynamic potential. This is the signature of a first-order phase transition. Consequently, the native and denatured states of a single-domain protein may be interpreted as two phases of a macroscopic system, which differ in structural order. For a single protein molecule the transformation can only be abrupt and not gradually. From this point of view a cooperative domain of a protein resembles a crystal, which has, however, a critical size, since it can only exist as a whole. Experimentally, however, one usually deals with protein ensembles.

The properties of the ensemble, which are reflected in the heterogeneity of the characteristic parameters of a protein, such as its energy, structure, compressibility, etc., render some specific features to the denaturing transition compared with phase transitions of thermodynamic systems: The transition is usually rather broad in the variables P or T (e.g., see Figures 5.9 and 5.10). This dispersion of the transition region is directly related to the heterogeneity of the protein ensemble, which has its roots in the fact that a protein, although a large molecule, is not an infinite

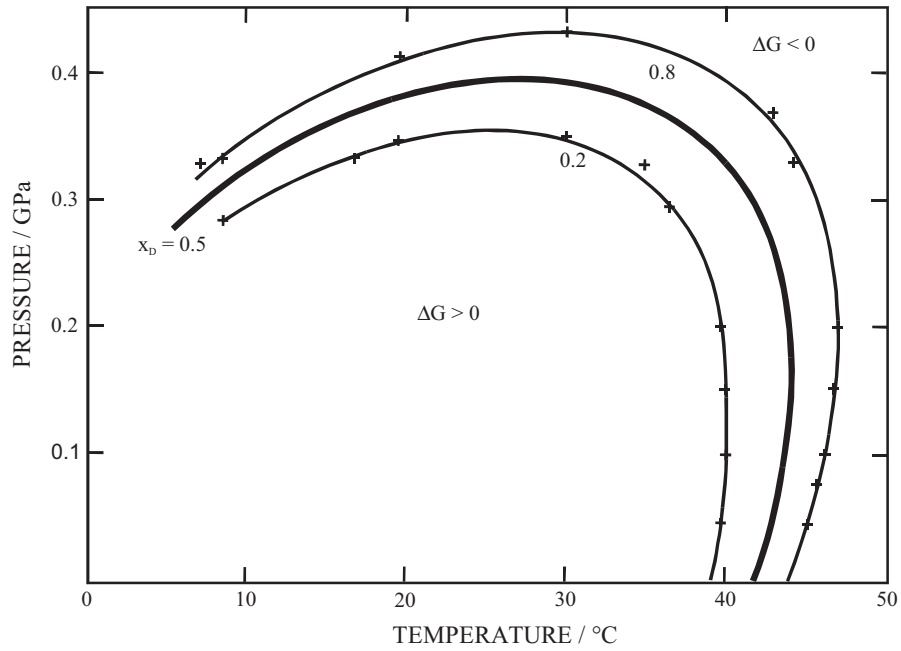

Fig. 5.2. Contours of constant chemical potential $\Delta\mu = \mu_D - \mu_N$ between the denatured (D) and the native (N) state of chymotrypsinogen (after Hawley [14]).

system. The equilibrium constant $K_{DN}(T, P)$ follows from the pressure analog of the van t'Hoff equation with $\partial T \rightarrow \partial P$ and $\Delta S \rightarrow -\Delta V$:

$$\partial(\ln K_{DN})/\partial P = -\Delta V/RT$$

The transition width, determined by the magnitude of the transition volume ΔV, is finite for a mesoscopic protein molecule, in contrast to the zero width of a macroscopic first-order transition.

Hawley, in 1971, was the first to interpret the curve on which the free energy difference between native and unfolded state vanishes as an elliptical phase boundary. This provided a natural explanation for the so-called re-entrant phase behavior of heat and cold denaturation [14]. Figure 5.2 shows the contours of the Gibbs free energy $\Delta G(P, T)$ versus pressure and temperature for chymotrypsinogen. Note that at moderate pressure levels (< 150 MPa), the temperature of heat denaturation increases slightly with pressure. Hence, applying pressure to the thermally denatured protein may actually drive the protein back into the native state. Upon further increasing the pressure, however, unfolding may occur again. In other words, the denatured phase is re-entered, irrespective of the fact that the pressure is monotonously changed. Phase diagrams with this property are called "re-entrant." A similar behavior is found if the temperature is changed. For instance, if one starts out at sufficiently high pressure levels (200 MPa) in the denatured

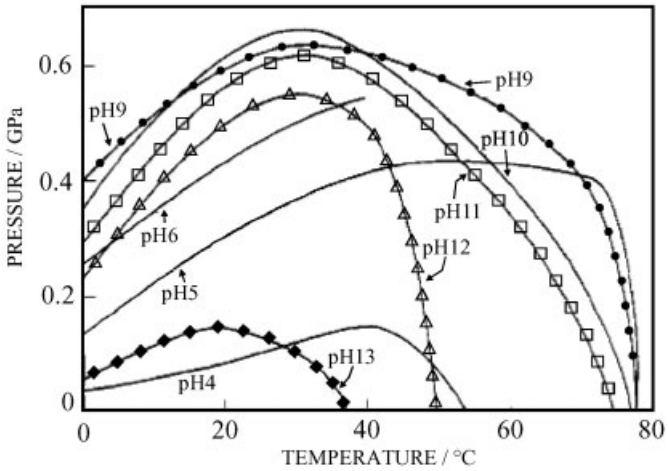

Fig. 5.3. Phase boundaries ($\Delta\mu = 0$) of myoglobin at various pH values, the native state is stable inside the contours, the denatured state outside (after Zipp and Kauzmann [18]).

state and lowers the temperature, one enters the native regime which is, however, left again at even lower temperatures to re-enter the denatured regime again. This latter transition is called ''cold denaturation''.

Re-entrant phase diagrams of perfect elliptical shape have been observed for liquid crystals by Cladis et al. [15] and by Klug and Whalley [16]. The elliptical shape was analyzed in detail by Clark [16].

In 1973, Zipp and Kauzmann, in a seminal paper, investigated the pressure–temperature–pH phase diagram of myoglobin [18]. They also observed re-entrant behavior, but did not attempt to fit the phase boundaries using ellipses. Depending on pH, the boundaries vary strongly in shape and show nonelliptical distortions, as shown in Figure 5.3.

In recent years, a significant number of studies HAVE suggested diagrams of elliptical shape for protein denaturation or for even more complex units, such as bacteria [19].

The stability phase diagram of proteins and related phenomena have been discussed in several review articles [20, 21].

Our goal is to eludicate the physical basis and thermodynamics of re-entrant protein phase diagrams, the conditions for elliptical shapes, and the limitations of this approach.

5.3
Thermodynamics of Pressure–Temperature Phase Diagrams

The phase equilibrium between the native and the denatured state N Φ D is controlled by the difference in the chemical potentials $\Delta\mu = \mu_D - \mu_N$. The ratio of con-

centrations of the denatured to the native form assuming a dilute solution is given by:

$$K_{DN} = c_D/c_N = \exp(-\Delta\mu/RT) \tag{1}$$

The chemical potential is the driving force that induces transport and transformations of a substance. It is analogous to the electrical potential, which can only induce currents because of charge conservation. Since the concentration of components, water, and protein is fixed (only pressure and temperature are varied), we restrict ourselves to one-component systems. The change $d\mu_i$ with temperature and pressure obeys the Gibbs–Duhem relation for each phase D and N:

$$\begin{aligned} d\mu_N &= -S_N\,dT + V_N\,dP = -RT\,d(\ln c_N/c_0) \\ d\mu_D &= -S_D\,dT + V_D\,dP = -RT\,d(\ln c_D/c_0) \end{aligned} \tag{2}$$

where S_N, S_D and V_N, V_D are the partial molar entropy and volume of the protein in solution in the native and denatured phase, respectively. Since entropy and volume are generally positive quantities, the chemical potential always decreases with increasing temperature, while it increases with increasing pressure, as shown in Figures 5.4 and 5.6. The potentials of two phases, differing in entropy, will thus cross at a particular temperature where a transition to the phase with the lower potential occurs. A similar change in phase will take place with pressure when the volumes of the two phases differ. Thus the more compact phase will be stable at high pressure.

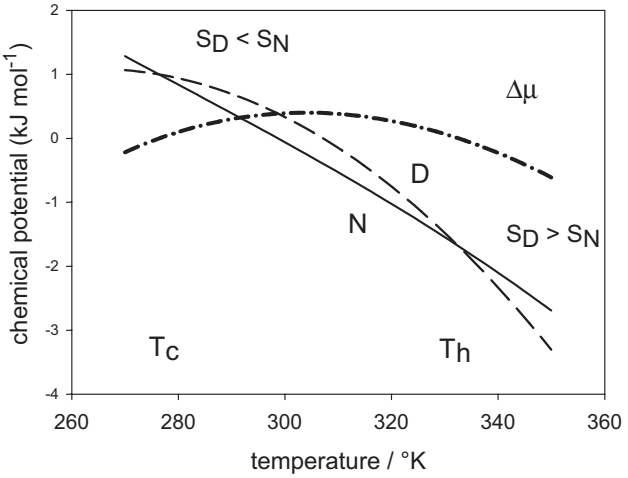

Fig. 5.4. The chemical potentials of the denatured (D) and the native (N) state of myoglobin and the resulting $\Delta\mu$ per mole of amino acid residue. Parameters [25]: ($\Delta\mu_{0N} = -0.2$ kJ mol^{-1}, $\Delta\mu_{0D} = 0.2$ kJ mol^{-1}, $S_C = 14$ kJ mol^{-1}, $\Delta C_p = 75$ kJ K^{-1} mol^{-1}). T_H, T_C, and T_M are the heat, cold denaturation temperature, and the temperature of maximum stability.

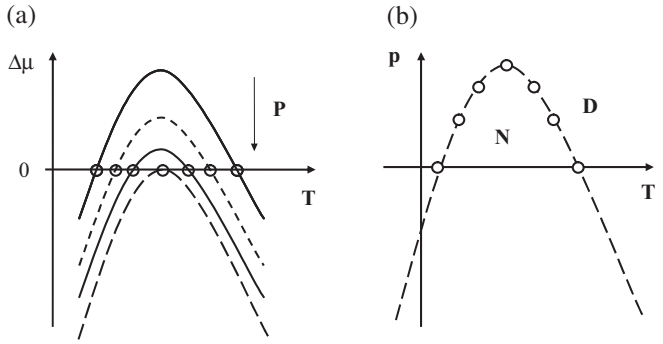

Fig. 5.5. a) Schematic representation of the difference $\Delta\mu = \mu_D - \mu_N$ of the chemical potential as a function of temperature for various pressures as deduced from Figure 5.4. b) The phase boundary as schematically deduced from the two $\Delta\mu = 0$ points of Figure 5.5a for negative values of $\Delta V = V_D - V_N$.

For proteins in particular, $S_D > S_N$ because of an excess in configurational entropy of the unfolded chain. Thus μ_D has the more pronounced temperature dependence and will fall below μ_N at T_H, the heat denaturation temperature. For myoglobin it is suggested in Figure 5.4 that the peculiar thermodynamic behavior of proteins arises from the strongly temperature-dependent entropy of the unfolded phase: the slope of $\mu_D(T)$ and thus the entropy $S_D(T)$ decrease with decreasing temperature.

On a microscopic scale this reflects the ordering force of nonpolar groups on surface water molecules. Since the corresponding hydrophobic effect is less pronounced in the native state, S_N is expected to be almost temperature independent. This discrepancy explains why the potential surfaces μ_D and μ_N meet again at T_C, the cold denaturation temperature as shown in Figure 5.4. The chemical potential difference, $\Delta\mu = \mu_D - \mu_N$, consequently assumes the shape of a convex curve, which is close to an inverted parabola with the maximum at T_M, the temperature of maximum stability (Figure 5.5).

Changes in pressure displace the difference potential surface $\Delta\mu$ vertically, depending on the unfolding volume ΔV as shown in Figure 5.5a.

Since the phase transition occurs at constant chemical potential, $\Delta\mu(P, T) = 0$, or $c_N = c_D$, while pressure and temperature are varied, one derives, from Eq. (2), a differential equation for the phase boundary, the Clausius–Claperon equation:

$$(dP/dT)_{\Delta\mu=0} = \Delta S/\Delta V \tag{3}$$

where $\Delta S = S_D - S_N$ and $\Delta V = V_D - V_N$ can depend on T and P. The phase boundary (Figure 5.5b) will assume the shape of an inverted parabola if the unfolding volume ΔV is negative and constant in P and T. For positive unfolding volumes a regular parabola, open to the high pressure side, would be obtained excluding denaturation by pressure.

The latent quantities ΔS and ΔV are composed of intrinsic contributions of the protein and those of the hydration shell, while the values of bulk water in both phases cancel.

The entropy difference reflects mainly the increase in configurational entropy of the chain, ΔS_C, and the entropy change ΔS_H in the hydration shell, due to exposure of buried residues. The same reasoning applies to the latent volume. Hence, we can write:

$$\begin{aligned} \Delta S &= \Delta S_C + \Delta S_H \\ \Delta V &= \Delta V_C + \Delta V_H \end{aligned} \tag{4}$$

We argue that the closed-phase boundaries displayed in Figures 5.2 and 5.3 are the consequence of the variation of ΔS_H and ΔV_H with temperature and pressure due to the hydrophobic effect. Exposure of nonpolar groups upon unfolding tends to immobilize water molecules, thereby decreasing their entropy. This mechanism is strongly temperature dependent. Its experimental signature is the positive heat capacity increment at constant pressure, $\Delta C_p > 0$, of the denatured relative to the native form. In simple terms, to increase the temperature of the unfolded phase requires additional entropy to continuously melt the immobilized water [8–10, 23, 24]. However, above a certain temperature, T_0, approximately 140 °C, the ordering effect has vanished.

Below T_0, the hydration entropy change, $\Delta S_H(T, T_0)$, is rapidly decreasing with decreasing temperature. Assuming ΔC_p to be approximately independent of temperature, one obtains for the change in "hydration entropy" [25]:

$$\Delta S_H(T) = \int_{T_0}^{T} \frac{\Delta C_P}{T} \mathrm{d}T = -\Delta C_P \cdot \ln\left(\frac{T_0}{T}\right) \tag{5}$$

and thus from Eqs (2)–(5):

$$\Delta\mu = \Delta\mu_0 - (T - T_0) \cdot [\Delta S_C - \Delta C_p \ln(T_0/T)] + \Delta V \cdot P \tag{6}$$

The hydration term $\propto \Delta C_p$ is always negative below T_0, stabilizing the denatured form. This is known as the "wedging effect" of water, which softens the native structure. The combined entropy difference ΔS vanishes at the maximum of $\Delta\mu$, at the temperature of maximum stability T_M (Figure 5.4):

$$(\partial\Delta\mu/\partial T)_{T=T_M} = -\Delta S = 0 \tag{7}$$

At T_M the negative hydration entropy ΔS_H just compensates for the positive configurational term ΔS_C:

$$\Delta S_C = \Delta C_p \ln(T_0/T_M) \tag{8}$$

ΔS in Eq. (7) depends on pressure and temperature according to:

$$d\Delta S(P,T) = (\partial \Delta S/\partial T)\,dT + (\partial \Delta S/\partial P)\,dP = (\Delta C_p/T)\cdot dT - \Delta\alpha_P \cdot dP = 0 \qquad (9)$$

where we have introduced the volume expansion increment $\Delta\alpha_P = (\partial \Delta V/\partial T)_{P=\text{const}}$.

Equation (9) defines the slope of a boundary $\Delta S(T,P) = \text{constant}$ in the P–T plane:

$$(dP/dT)_{\Delta S=\text{const}} = \Delta C_p/(T\cdot\Delta\alpha_P) \qquad (10)$$

The special $\Delta S = 0$ line, separating regions of positive and negative transition entropies, is fixed by the condition $(dP/dT)_{\Delta\mu=0} = 0$ as shown in Figure 5.11. Since the slope in Figure 5.11 is positive and since both ΔC_p and ΔV are positive, it follows that $\Delta\alpha_P > 0$. Integrating Eq. (10) yields the effect of pressure on the temperature of maximum stability:

$$T_M = T_{M0}\cdot\exp(P\cdot\Delta\alpha_p/\Delta C_p) \qquad (11)$$

For reasonably low pressures one has for the $\Delta S = 0$ line: $T_M \approx T_{M0}\cdot(1 + P\cdot\Delta\alpha_p/\Delta C_p)$. Expanding the chemical potential (Eq. (6)) about $T_M \approx T_{M0}$ yields an approximate parabola in T with negative curvature (Figure 5.5a):

$$\Delta\mu(T,P) = \Delta\mu_M - \tfrac{1}{2}\Delta C_p\cdot(T - T_M)^2/T + \Delta V\cdot P = -RT\ln(c_D/c_N) \qquad (12)$$

For $\Delta V < 0$, increasing pressure diminishes the stability range of the native state. If ΔV is constant, one obtains the parabolic pressure–temperature phase diagram, $P(T)_{\Delta\mu=0}$, shown in Figure 5.5b.

Experimental data, like those shown in Figure 5.2, 5.3, and 5.11 suggest a reentrant phase behavior not only as a function of temperature but also as a function of pressure. This leads to a closed or ''ellipsoidal'' phase boundary with ΔV depending on pressure and temperature. The volume of the denatured form, the slope of $\mu_D(P)$ in Figure 5.6, which increases with decreasing pressure. Thus a second crossing of the D–N potentials may occur at low or even negative pressure denoted by P_L. Thus the unfolded protein is more easily stretched than the compact native state. Moreover, near $P = 0$, a pressure increase will stabilize the native state. In analogy to the temperature (Eq. (7)) we can define a pressure of maximum stability, P_M, according to:

$$(\partial\Delta\mu/\partial P)_{P=P_M} = \Delta V = 0 \qquad (13)$$

Combining Eqs (4) and (13) shows that the changes in configurational and hydration volume cancel at $P = P_M$. The small observed unfolding volumes may result from such compensation effects. Equation (13) allows determination of the $\Delta V(P,T) = 0$ line, separating regions of positive and negative volume changes:

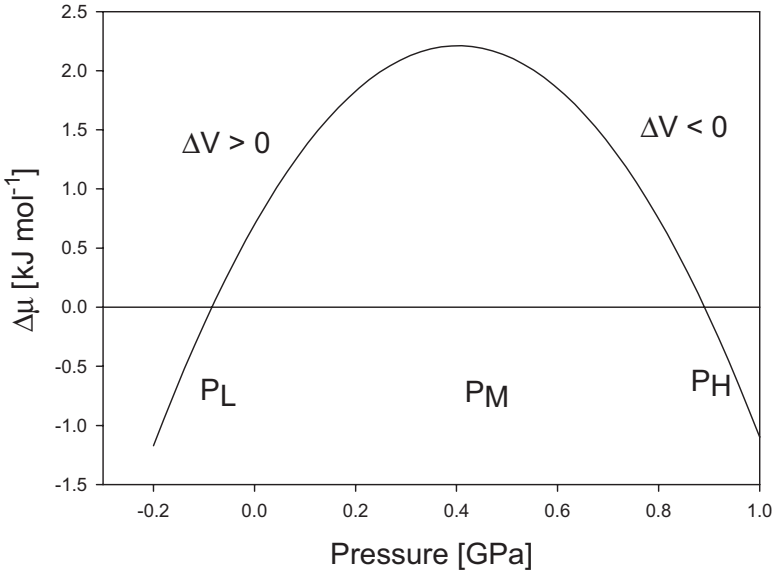

Fig. 5.6. Effect of pressure on the chemical potential $\Delta\mu$ for the parameters of cytochrome *c* at 280 K (Table 5.1 and Eq. (17)). The volume of the denatured state decreases with pressure to below the value of the native protein, which leads to a crossing at high pressure P_H. A second crossing occurs at negative pressure P_L. P_M is the pressure of maximum stability.

$$(\partial\Delta V/\partial T)\,\mathrm{d}T + (\partial\Delta V/\partial P)\,\mathrm{d}P = \Delta\alpha_P \cdot \mathrm{d}T - \Delta\beta_T \cdot \mathrm{d}P = 0 \tag{14}$$

thus

$$(\mathrm{d}P/\mathrm{d}T)_{\Delta V=\mathrm{const}} = \Delta\alpha_P/\Delta\beta_T \tag{15}$$

The $\Delta V = 0$ line follows from the additional condition: $(\mathrm{d}P/\mathrm{d}T)_{\Delta\mu=0} = \propto$. For the pressure of maximum stability one obtains:

$$P_M = P_r + (\Delta\alpha_P/\Delta\beta_T)(T - T_r) \tag{16}$$

$\Delta\beta_T$ denotes the increment in the compressibility coefficient: $\Delta\beta_T = -(\partial\Delta V/\partial P)$. T_r denotes an unspecified reference temperature. For second-order phase transitions, sometimes associated with molten globule denaturation [26, 27], there is no discontinuity in the extensive quantities.

Equations (9) and (14) then become the so-called Ehrenfest equations: $(\mathrm{d}P/\mathrm{d}T)_{\Delta S=0} = (\mathrm{d}P/\mathrm{d}T)_{\Delta V=0}$

For most proteins cold denaturation occurs at subzero temperatures in the unstable or supercooled region of the water phase diagram. For this reason cold denaturation was formerly considered to be irrelevant to protein science. Similarly, low-pressure denaturation at $P_L(T)$ occurs for most proteins in a large temperature

range where pressure is negative. Liquids under tension are unstable, although metastable states can exist, since the creation of a new liquid–gas interface involves the crossing of an energy barrier. The first experiments were performed by Berthelot in 1850 using a spinning capillary [28]. Stretched states of water at pressures as low as –280 bars have been observed using the same method [29]. Unfolding experiments with protein solutions at negative pressures still need to be performed. The folding of unstable proteins such as nuclease conA remains incomplete at positive pressure, while negative pressure may further stabilize the native state [30]. At sufficiently high temperature, low-pressure denaturation may occur in the positive range (Figure 5.11) and in this case it is easily accessible experimentally.

Pressure- and temperature-dependent transition volumes originate from finite increments in the partial compressibility $\Delta\beta_T$ and the volume expansion coefficient $\Delta\alpha_P$. Expanding the latent volume ΔV about a reference point (T_r, P_r) yields:

$$\Delta V(P,T) = \Delta V_r - \Delta\beta_T \cdot (P - P_r) + \Delta\alpha_P \cdot (T - T_r) \tag{17}$$

The major part of the change in the compressibility upon global transformations of proteins is due to hydration processes [31]. The greater the hydration, the smaller the partial compressibility. This is the rule for protein solutions at normal temperature and pressure. For native proteins the intrinsic compressibility is as low as that of organic solids [32–34]. The outer surface contribution to the measured partial compressibility is quite negative. Thus complete unfolding leads to a considerable decrease in the partial compressibility due to the loss of intramolecular voids and the expansion of the surface area contacting the bulk water [35]. In this low pressure/high temperature regime $\Delta\beta_T$ is negative, while $\Delta\alpha_P$ is mostly positive. This results in a positive unfolding volume (Eq. (17)) as indicated in Figure 5.6. Consequently moderate pressures stabilize the native state. A number of studies suggest that high-pressure denaturation leads to incomplete unfolding and structures resembling those of molten globule states (MG) [5–7, 36]. The N → MG transition is generally accompanied by an increase in compressibility. The tendency towards a positive $\Delta\beta_T$ at higher pressures due to partial unfolding may lead to the observed negative unfolding volumes. Combining Eqs (12) and (17), the phase boundary $\Delta\mu(T, P) = 0$ with respect to a reference point (T_r, P_r) assumes the form of a second-order hyperface:

$$\begin{aligned} &-\tfrac{1}{2}\Delta C_p \cdot (T - T_r)^2/T - \tfrac{1}{2}\Delta\beta_T \cdot (P - P_r)^2 + \Delta\alpha_P \cdot (T - T_r) \cdot (P - P_r) \\ &\quad - \Delta S_r \cdot (T - T_r) + \Delta V_r \cdot (P - P_r) + \Delta\mu_r = 0 \end{aligned} \tag{18}$$

For approximately constant increments $\Delta C_p, \Delta\beta_T, \Delta\alpha_P$, the phase boundary assumes parabolic ($\Delta\beta_T = 0$), hyperbolic or closed elliptical shapes. The basic condition to obtain an elliptical phase diagram is given by:

$$(\Delta C_p)(\Delta\beta_T) - (\Delta\alpha_P)^2 > 0 \tag{19}$$

Since experiments show that $\Delta C_p > 0$, Eq. (19) requires the compressibility change to be positive: $\Delta\beta_T > 0$. A hyperbolic shape would imply a negative left-hand side in Eq. (19). Thus far only elliptical diagrams, in some cases with distortions (e.g., Figure 5.3) have been discussed. A complete solution would require data in the range where pressure is negative: the data shown in Figure 5.2 are also consistent with a parabolic shape.

5.4 Measuring Phase Stability Boundaries with Optical Techniques

5.4.1 Fluorescence Experiments with Cytochrome *c*

Protein denaturing processes can be investigated with many techniques. The most convenient ones concerning the determination of the whole stability diagram are spectroscopic techniques. Almost all methods have been used: IR, Raman, NMR, absorption and fluorescence spectroscopy. However, data covering complete phase diagrams are quite rare. Some of them were reviewed above. The various techniques have their specific advantages as well as disadvantages. For instance, with vibrational spectroscopy one obtains information on structural changes such as the weakening of the amide I band [20, 21, 37, 38], with NMR one obtains information on hydrogen exchange and the associated protection factors [6] from which conclusions on structural details of the denatured state can be drawn. However, as a rule no information on the structure disrupting mechanism under pressure is obtained. The situation with absorption and fluorescence spectroscopy is different. In optical spectroscopy it is the spectral position and the linewidth of an electronic transition that is measured. From these quantities it is, as a rule, quite difficult to extract any structural information. On the other hand, one obtains detailed information on the interaction of the electronic states with the respective environment. Since these interactions are known in detail, it is possible to extract from their behavior under pressure and temperature changes information on the mechanism of phase crossing.

Compared with other spectroscopic techniques, fluorescence spectroscopy is also the most sensitive. Hence, it is possible to work at very low concentration levels so that aggregation processes can easily be avoided. In most experiments tryptophan is used as a fluorescent probe molecule. With chromoproteins this is, generally speaking, impossible since fast energy transfer to the chromophore quenches the UV fluorescence to a high degree. In the following we describe fluorescence experiments on a cytochrome *c*-type protein in a glycerol/water matrix [39]. The native heme iron was substituted by Zn in order to make the protein strongly fluorescent in the visible range. As a short notation for this protein we use the abbreviation Zn-Cc.

The set-up for a fluorescence experiment is simple and is shown in Figure 5.7.

The sample is in a temperature- and pressure-controlled diamond anvil cell.

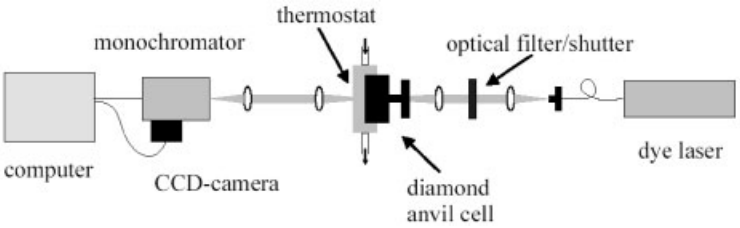

Fig. 5.7. Sketch of a fluorecence experiment for measuring the phase diagram of proteins.

Pressure can be varied up to about 2 Gpa. Its magnitude is determined from the pressure shift of the ruby fluorescence, for which reference values can be taken from the literature [40]. The temperature is controlled by a flow thermostat between −20 °C and 100 °C. Excitation is carried out into the Soret band at 420 nm with light from a pulsed dye laser pumped by an excimer laser. The fluorescence is collected in a collinear arrangement, dispersed in a spectrometer and detected via a CCD camera. The quantities of interest for measuring the protein stability phase diagram are the spectral position and the width of the $S_1 \rightarrow S_0$ 00-transition (587 nm, Figure 5.8). Generally speaking the spectral changes for Zn-Cc are rather small. Nevertheless the measured changes of the spectral shifts and widths are accurate within about 3%. Figure 5.8 shows the fluorescence spectrum of Zn-Cc between 550 and 700 nm as it changes with pressure. The sharp line around 695 nm is the fluorescence from ruby.

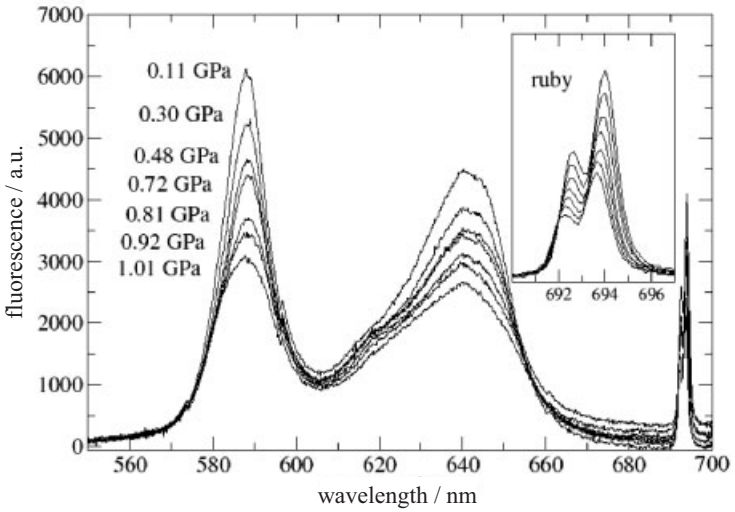

Fig. 5.8. Fluorescence spectrum of Zn-cytochrome *c* in glycerol/water at ambient temperature as it changes with pressure. The stability diagram was determined from the changes of the first and second moment of the 00-band at 584 nm. The fluorescence from ruby is shown as well. It serves for gauging the pressure.

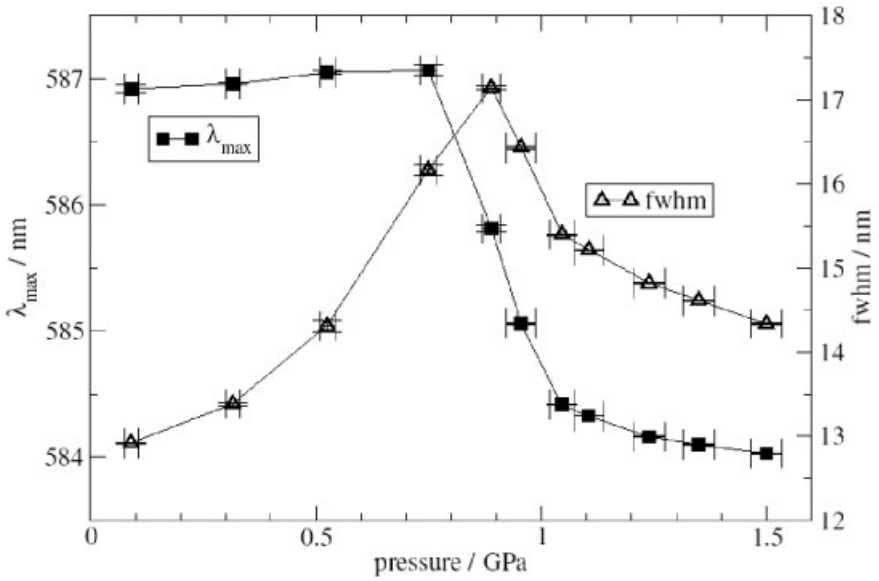

Fig. 5.9. The behavior of first and second moment of the fluorescence under pressure variation at ambient temperature.

5.4.2 Results

Figures 5.9 and 5.10 show typical results for the changes in the first and second moment (position of the maximum and width) of the 00-band under pressure and temperature variation.

If pressure is increased the band responds with a red shift, although a very small one (Figure 5.9). Around 0.75 GPa the red shifting regime changes rather abruptly into a blue shifting regime which levels off beyond 1 GPa. A qualitatively similar behavior is observed for the band shift under a temperature increase: a red shifting phase (in this case more pronounced) is followed by a blue shifting phase (Figure 5.10). Quite interesting is the behavior of the bandwidth: an increase of pressure leads to a rather strong increase in the width (Figure 5.9). This is the usual behavior and just reflects the fact that an increase in density results in an increase in the molecular interactions due to their strong dependence on distance. However, if the pressure is increased beyond about 0.9 GPa, the band all of a sudden narrows. This narrowing levels off beyond about 1 GPa. As can be seen from the figure, the maximum in the bandwidth coincides with the midpoint of the blue shifting regime. The thermal behavior of the bandwidth is different (Figure 5.10): there is no narrowing phase, but there is kind of a kink in the increase of the bandwidth with temperature around 65 °C. Again, this change in the thermal behavior of the width

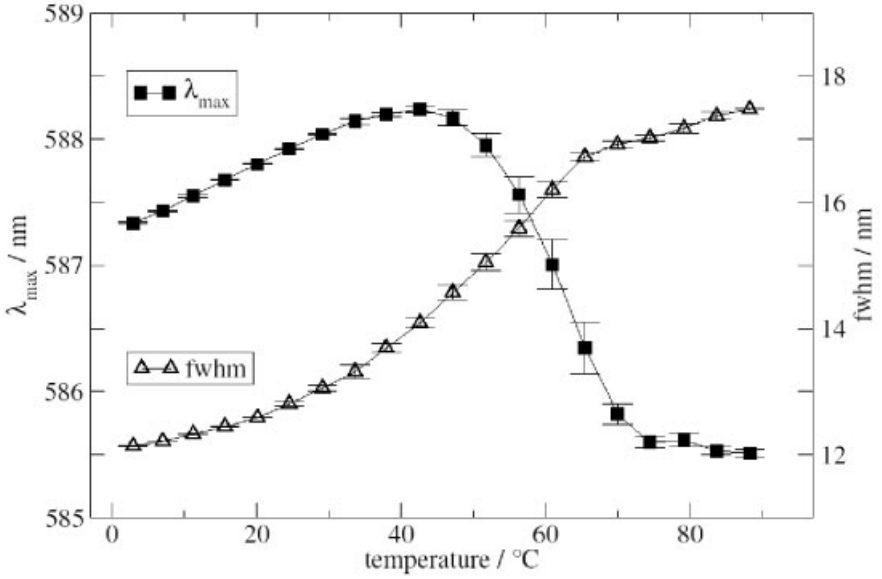

Fig. 5.10. The behavior of the first and second moment of the fluorescence under temperature variation at ambient pressure.

coincides rather well with the midpoint in the thermally induced blue shifting phase.

For measuring the complete phase diagram we performed a series of pressure scans from ambient pressure up to about 1.5 GPa at various temperatures and a series of temperature scans from a few centigrades up to about 90 °C at various pressure levels. The respective pattern of the changes of the fluorescence always showed the sigmoid-like behavior as discussed above. We associate the midpoint of the blue shifting regime with the stability boundary between the native and the denatured state of the protein due to reasons discussed below.

The complete stability diagram is shown in Figure 5.11. The solid line represents an elliptic least square fit to the experimental points. The two solid lines $\Delta S = 0$ and $\Delta V = 0$ cut the stability diagram at points where the volume and the entropy difference change sign (see also Eqs (11) and (16)). For instance, for all data points to the left of the $\Delta S = 0$ line the entropy in the denatured state S_D is smaller than S_N, the entropy in the native state (see below).

Figures 5.12 and 5.13 show specific features of the fluorescence behavior which we want to discuss separately. Figure 5.12 shows the behavior of the first and second moment for cold denaturation at ambient pressure. The point which we want to stress is that the band shift no longer reflects the qualitative change in its behavior. Instead, we observe a blue shift which increases in a nonlinear fashion with decreasing temperature. From such a behavior it is hard to determine a transition

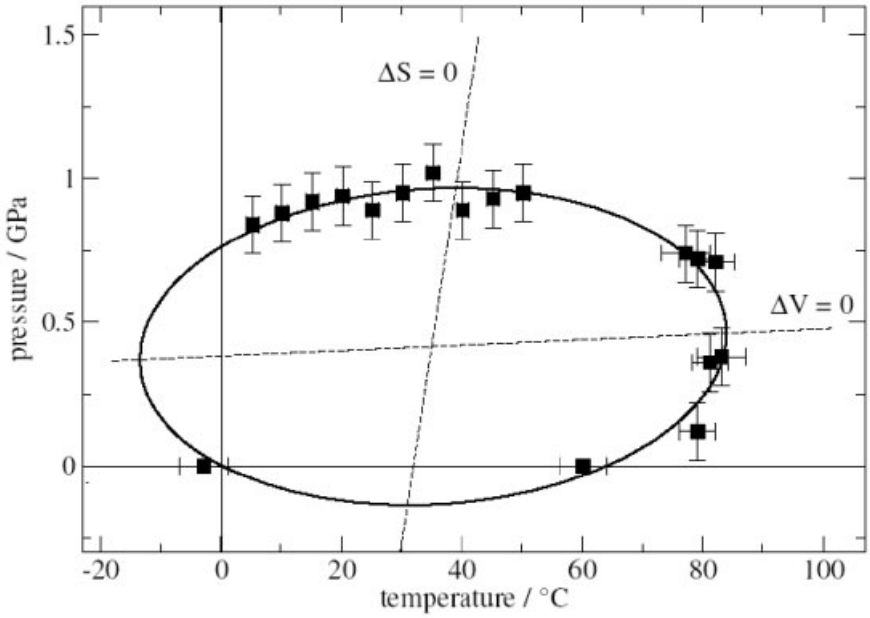

Fig. 5.11. The stability phase diagram of Zn-cytochrome *c*. The solid line is an elliptic least square fit to the data points. The straight lines mark the points where ΔS and ΔV change sign.

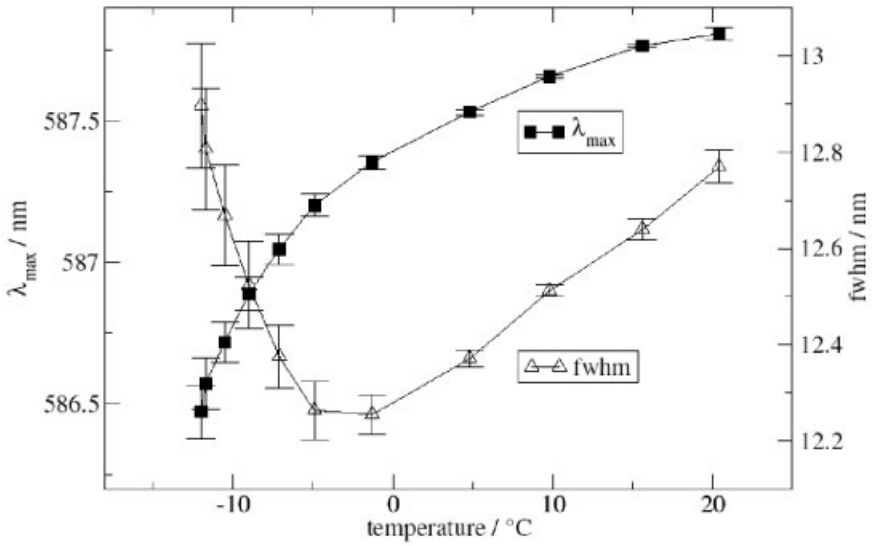

Fig. 5.12. The behavior of the first and second moment of the fluorescence for cold denaturation at ambient pressure.

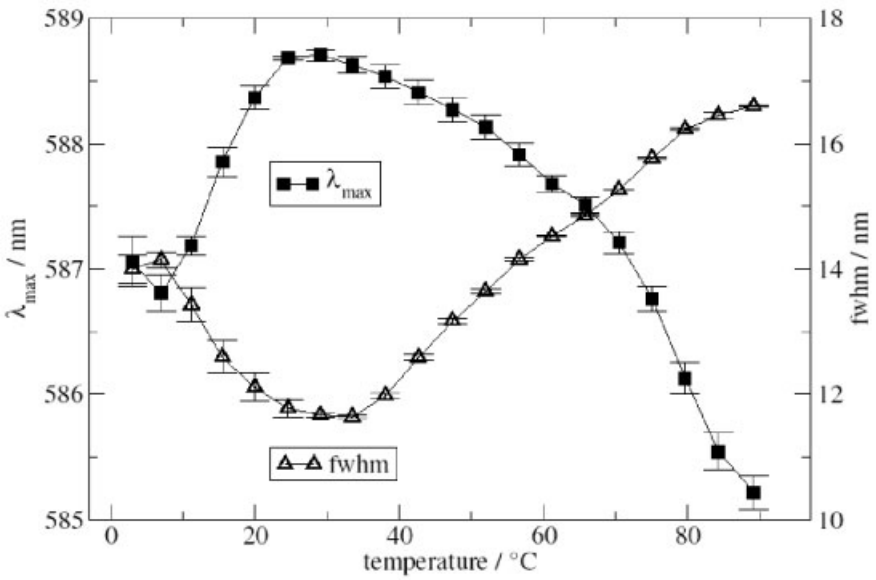

Fig. 5.13. The first and second moment of the fluorescence under a temperature variation at high pressure (0.7 GPa). The pattern shows features characteristic for re-entrant phase crossing.

point. The bandwidth, on the other hand, shows a quite unusual behavior: it narrows with decreasing temperature, but around −3 °C it runs through a minimum and starts broadening upon further decreasing the temperature. The unusual behavior concerns the broadening with decreasing temperature. This broadening obviously originates from an additional state which becomes populated below −3 °C. Naturally, this state must be the denatured state of the protein. Hence, we associate this minimum in the bandwidth with the stability boundary.

The temperature dependence of the moments in Figure 5.13 follows a rather complex pattern. This pattern comes from the re-entrant character of the phase diagram which has been stressed in Section 5.2. At a pressure level of 0.7 GPa, the protein is denatured to a high degree if the temperature is below around 10 °C (see Figure 5.11). Hence, upon increasing the temperature, the protein enters the stable regime. This is most clearly reflected in a narrowing of the bandwidth due to the fact that the denatured state becomes less and less populated At the same time the band maximum undergoes a red shift in line with the observation that the denatured state is blue shifted from the native one. However, around 25 °C the red shifting phase turns into a blue shifting phase, signaling that the protein re-enters the denatured regime. The bandwidth data support this conclusion. Interestingly, the data convey the impression that there are more than just two transitions involved; their nature, however, is not clear.

5.5
What Do We Learn from the Stability Diagram?

5.5.1
Thermodynamics

The eye-catching feature in Figure 5.11 is the nearly perfect elliptic shape of the stability diagram in agreement with the simple model developed in Section 5.3. The elliptic shape implies that the characteristic thermodynamic parameters of the protein, namely the increments of the specific heat capacity, the compressibility and the thermal expansion are rather well-defined material parameters, i.e., do not significantly depend on temperature and pressure. In addition, since the model is based on just two states, we conclude from the elliptic shape that the protein investigated, namely Zn-Cc, can be described as a two-state folder. Applying the Clausius–Clapeyron equation (Eq. (3)) to the elliptic phase boundary, we see that there are distinct points characterized by $(\mathrm{d}P/\mathrm{d}T)_{\Delta\mu=0} = \infty$ and by $(\mathrm{d}P/\mathrm{d}T)_{\Delta\mu=0} = 0$. The former condition separates the regime with positive ΔV from the regime with negative ΔV. The latter one separates the regime with positive ΔS from the regime with negative ΔS (Eqs (7) and (13)).

Let us consider thermal denaturation at ambient pressure. ΔS is definitely positive because the entropy of the chain increases upon denaturation and the entropy of the solvent increases as well. Since the slope of the phase boundary is positive, ΔV must be positive, too. However, moving along the phase boundary, we eventually cross the $\Delta V = 0$ line. For all points above that line, ΔV is negative. In other words: application of pressure destabilizes the native state and favors the denatured state. Below the $\Delta V = 0$-line, ΔV is positive. Accordingly, application of pressure favors the native state.

In a similar way, for all points to the right of the $\Delta S = 0$ line, ΔS is positive. A positive entropy change upon denaturation is what one would straightforwardly expect. However, to the left of the $\Delta S = 0$ line, the entropy change is negative, meaning that the entropy in the denatured state is smaller than in the native state. As was discussed above, the negative entropy change is due to an upcoming ordering of the hydration water as the temperature is decreased: The exposure of hydrophobic groups causes the water molecules in the hydration shell to become more and more immobilized due to the formation of a stronger hydrogen network. Right at the point where the $\Delta S = 0$ line cuts the phase diagram, the chain entropy and the entropy of the hydration shell exactly cancel, as we have stressed above.

There is another interesting outcome from the elliptic shape of the phase diagram: Eq. (19) tells us that the change in the compressibility upon denaturation has to have the same sign as the change in the specific heat. The change in the specific heat is positive meaning that the heat capacity is larger in the unfolded state. As outlined above, this is due to the fact that an increase of the temperature in the denatured state requires the melting of the ordered immobilized hydration shell. Accordingly, $\Delta\beta$ has to be positive, meaning that the compressibility in the denatured state is larger than in the native state. As to the absolute values of

the thermodynamic parameters which determine the phase diagram, they can be determined only if one of the parameters is known. In the following section we will show how the equilibrium constant can be determined as a function of temperature and pressure and how this can be exploited to extract the thermodynamic parameters on an absolute scale.

5.5.2 Determination of the Equilibrium Constant of Denaturation

The body of information that can be extracted from the thermodynamics of protein denaturation reveals surprising details. However, it should be stressed again that all the modeling is based on two important assumptions, namely that folding and denaturing is described within the frame of just two states, N and D, and that these two states are in thermal equilibrium. Neither of these assumptions is straightforward. It is well known that the number of structural states, even of small proteins is, is extremely large [41–47] and the communication between the various states can be very slow so that the establishment of thermal equilibrium is not always ensured. We understand the two-state approximation on the basis of a concept which we call ''state lumping.'' In simple terms this means that the structural phase space can be partitioned into two areas comprising, on the one hand, all the states in which the protein is functioning and, on the other hand, the area in which the protein is dead. We associate the native state N and the denatured state D with these two areas. In order for the ''state lumping'' concept to work, the immediate consequence is that all states within the two and between the two areas are in thermal equilibrium. Whether this is true or not can only be proven by the outcome of the experiments.

For Zn-Cc this concept seems to hold sufficiently well. In our experiments, typical waiting times for establishing equilibrium were of the order of 20 minutes. In order to make sure that this time span is reasonable, we measured for some points on the phase boundary also the respective kinetics. However, we also stress that at high pressures and low temperatures (left side of the phase diagram, Figure 5.11) we could not get reasonable data and we attributed this to the fact that equilibrium could not be reached within the experimental time window.

Assuming that equilibrium is established and the two-state approximation holds with sufficient accuracy, we can determine the equilibrium constant as a function of pressure and temperature from the fluorescence experiments and from the fact that the phase diagram has an elliptic shape. We proceed in the following way: The fluorescence intensity $F(\lambda)$ in the transformation range is a superposition from the two states N and D with their respective fluorescence maximum at λ_N and λ_D:

$$F(\lambda) = p_N a_N \exp[-(\lambda - \lambda_N)^2/2{\sigma_N}^2] + p_D a_D \exp[-(\lambda - \lambda_D)^2/2{\sigma_D}^2] \quad (20)$$

where p_N and p_D are the population factors of the two states N and D, a_N and a_D are the respective oscillator strengths. Changes of the temperature or the pressure of the system cause a change in the population factors p_N and p_D which, in turn,

leads to a change in the first moment of $F(\lambda)$, that is in the spectral position of the band maximum, λ_{max}. As to Zn-Cc, we can make use of some of its specific properties: First, the chromophore itself is quite rigid, hence, it is not likely affected by pressurizing or heating the sample. Accordingly, it is safe to assume that the oscillator strengths in the native and in the denatured state are not significantly different from each other. Second, the spectral changes induced by varying the temperature or the pressure are rather small compared to the total width of the long wavelength band (Figure 5.8). In addition, the wavelengths λ_N and λ_D are rather close and well within the inhomogeneous band. As a consequence, the exponentials in Eq. (20) are roughly of the same magnitude irrespective of the value of λ. Along these lines of reasoning, λ_{max} is readily determined from the condition $dF/d\lambda = 0$:

$$\lambda_{max} = p_N(T,P)\lambda_N + p_D(T,P)\lambda_D = p_N(T,p)[\lambda_N - \lambda_D] - \lambda_D \qquad (21)$$

The last term on the right hand side of Eq. (21) holds because we restrict our evaluation to an effective two-state system. According to the above equation, the band maximum in the transition region is determined by a population weighted average of λ_N and λ_D. Since λ_N and λ_D depend on pressure and temperature themselves, we have to determine the respective edge values in the transition region. How this is done is shown in Figure 5.14 for thermal denaturation at ambient pressure. Similar figures are obtained for any parameter variation. Having λ_{max} as a function of pressure or temperature from the experiment and knowing the respective edge

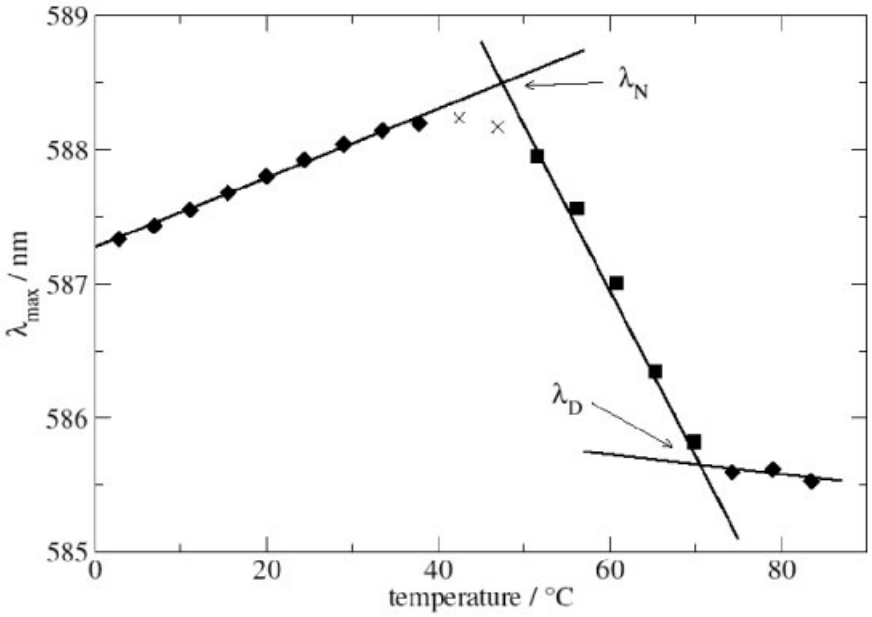

Fig. 5.14. Determination of the edge values λ_N and λ_D.

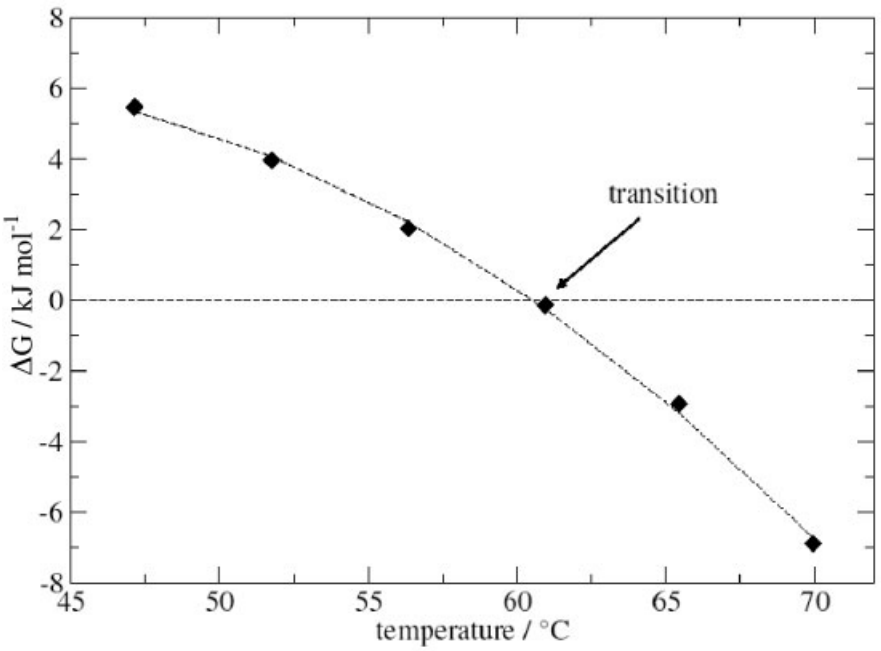

Fig. 5.15. Temperature dependence of the difference of the Gibbs free energy ΔG. (Note that, for a one-component system, $\Delta G/\mathrm{Mol} = \Delta\mu$).

values λ_N and λ_D, the population factors p_N and p_D can readily be evaluated as a function of pressure and temperature using Eq. (21). From the population factors the equilibrium constant K follows immediately:

$$K_{DN}(T,P) = [1 - p_N(T,P)]/p_N(T,P) \tag{22}$$

Once K is known, $\Delta\mu$ (or, equivalently, $\Delta G\ \mathrm{mol}^{-1}$) can be determined as a function of pressure and temperature from Eq. (1). For a fixed pressure, say p_i, $\Delta\mu(T, P_i)$ forms an inverted parabola in T, as was shown in Section 5.3. The same is true for $\Delta\mu(P, T_i)$. So we determined $\Delta\mu(T)$ and $\Delta\mu(P)$ by fitting parabolas to the few data points (Figures 5.15 and 5.16) under the constraints that both branches of these parabolas have to go through the phase boundaries of the stability diagram (Figure 5.11). From the first and second derivative of $\Delta\mu$ with respect to temperature and pressure all the thermodynamic parameters, namely $\Delta V(T,P), \Delta S(T,P)$, $\Delta C_p, \Delta\beta$ and $\Delta\alpha$, can be determined. For Zn-Cc this parameters are listed in Table 5.1. We took ΔC_p from the equilibrium constant because it seems to be the most accurate parameter (Figure 5.15). As a matter of fact our value is rather close to what was measured by Makhatadze and Privalov for unfolding native cytochrome c [10]. All the other parameters are determined from the phase diagram. Note that $\Delta\beta$ has the same sign as ΔC_p, as required for an elliptic shape of the diagram.

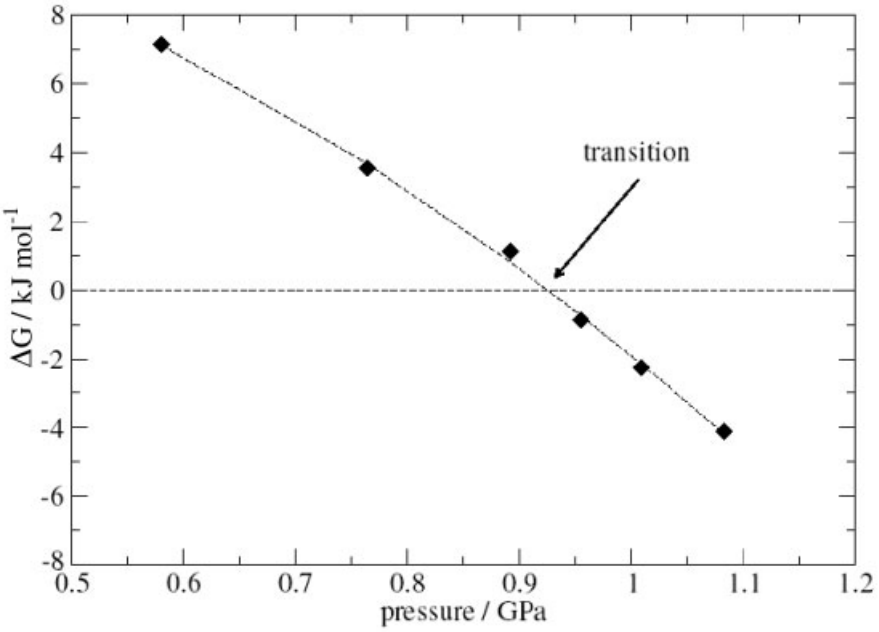

Fig. 5.16. Pressure dependence of the difference in the Gibbs free energy ΔG.

5.5.3 Microscopic Aspects

Having determined the complete set of thermodynamic parameters which govern denaturation of Zn-Cc, we may now proceed with exploring the microscopic driving forces of denaturation. We stress that the pattern in the behavior of the first moment of the fluorescence 00-transition is qualitatively very similar for thermal and pressure denaturation: A red shifting regime upon an increase in both parameters is followed by a blue shifting regime which signals the onset of the transformation range. The solvent shift of an optical transition is mainly determined by

Tab. 5.1. Thermodynamic parameters for the denaturation of Zn-cytochrome *c*.

Parameters	*From the fit*
ΔC_p (kJ mol^{-1} K^{-1})	5.87
$\Delta\beta$ (cm^3 mol^{-1} GPa^{-1})	148.1
$\Delta\alpha$ (cm^3 mol^{-1} K^{-1})	0.139
ΔV (0.91 GPa, 298 K) (cm^3 mol^{-1})	−74.6
ΔS (0.91 GPa, 298 K) (kJ mol^{-1} K^{-1})	−0.263
ΔV (0.1 MPa, 333 K) (cm^3 mol^{-1})	65.0
ΔS (0.1 MPa, 333 K) (kJ mol^{-1} K^{-1})	0.530

two types of interactions, namely the dispersive and the higher order electrostatic interaction (dipole–induced dipole). Both types of interaction are very short ranged. They fall off with distance R as R^{-6}. From the pioneering papers by Bayliss, McRae and Liptay [48–50], it is well known that the dispersive interaction is always red shifting because the polarizability in the excited state is higher than in the ground state. However, electrostatic interactions can cause shifts in both directions, to the red as well as to the blue, depending on how the dipole moment of the chromophore changes in the excited state compared with the ground state Accordingly, in the blue shifting regime, the electrostatic interaction of the probe with its environment obviously increases compared with the dispersive interaction. As a consequence, we conclude that polar groups with a sufficiently large dipole moment have to come close to the chromophore to induce this shift.

As to thermal denaturation, such an interpretation seems to fit quite well into the scenario. Baldwin [23], for instance, could show that thermal denaturation of a protein is remarkably well described in analogy to the solvation of liquid hydrocarbons in water. This ''oil droplet model'' accounts for the temperature dependence of the hydrophobic interaction: The entropic driving force for folding, which comprises the major part of the hydrophobic interaction, decreases as the temperature increases. This driving force is associated with the formation of an ordered structure of the water molecules surrounding the hydrophobic amino acids. At sufficiently high temperature this ordered structure melts away so that the change of the unfolding entropy of the polypeptide chain takes over and the protein attains a random coil-like shape [5]. Since a random coil is an open structure, the chromophore may now be exposed to water molecules. Water molecules have a rather high permanent dipole moment, hence, may become polarized through the electrostatic interaction with the chromophore. Along these lines of reasoning, it seems straightforward that the observed blue shifting regime of the fluorescence in the thermal denaturation of Zn-Cc comes from the water molecules of the solvent. However, as was pointed out by Kauzmann [51], the ''oil droplet model'' has severe shortcomings, despite its success in explaining the specific features of thermal denaturation. It almost completely fails in explaining the specific features of pressure induced denaturation. Pressure denaturation is governed by the volume change ΔV (Section 5.3). In this respect hydrophobic molecules behave quite differently from proteins: ΔV for protein unfolding is negative above a few hundred MPa (see, for instance, Figure 5.11 and discussions in Sections 5.3 and 5.5.1), whereas it is positive in the same pressure range for transfering hydrophobic molecules into water. There are two possible consequences: Either the ''oil droplet model'' is completely wrong, or the pressure denatured state is different from the thermally denatured state.

Indeed, Hummer and coworkers could show that the latter possibility is true [52, 53]. On the basis of their calculations they suggested that, as pressure is increased, the tretrahedral network of H-bonds in the solvent becomes more and more frustrated so that the pressure-induced inclusion of water molecules within the hydrophobic core becomes energetically more and more favorable. As a consequence, the contact configuration between hydrophobic molecules is destabilized by pressure

whereas the solvent-separated contact configuration (a water molecule between two hydrophobic molecules) is stabilized. In simple words this means that water is pressed into the protein, the protein swells but does not completely unfold into a random coil conformation but rather seems to retain major parts of its globular shape. The important conclusion is that pressure denaturation is based on the presence of water. Larger solvent molecules, such as glycerol, can obviously not penetrate the protein, hence may act as stabilizing elements against pressure [54].

It seems that this view on the microscopic aspects of pressure denaturation is convincingly supported by our experiments: First, we stress again that the general pattern in the variation of the first moment with pressure is very similar to the respective variation with temperature. Since, in the latter case, we attributed this pattern to water molecules approaching the chromophore, it is quite natural to associate the pressure-induced pattern with the same phenomenon. Second, the magnitude of the change in the first moments is about the same for thermally and pressure-induced denaturation. Accordingly, the change in the respective interaction has to be very similar. This means, that, on average, the number and the distances of the additionally interacting water molecules have to be the same.

In order to get additional support for this reasoning we performed pressure tuning hole burning experiments [55]. With these experiments it is possible to estimate the size of an average interaction volume of the chromophore with its environment. We found that the respective radius is about 4–5 Å. Accordingly, application of high pressure forces water molecules from the hydration shell into the interior of the protein where they fill the voids around the chromophore in the heme pocket. High-pressure (0.9 GPa) MD simulations (M Reif and Ch Scharnagl, in preparation) are in full agreement with this view of pressure denaturation.

Summarizing this section we state that fluorescence experiments in combination with other optical experiments and computer simulations provide a detailed insight into the processes involved in pressure-induced protein denaturation.

5.5.4 Structural Features of the Pressure-denatured State

From the discussion above it is evident that pressure denaturation leads to a structural state which is different from the respective one obtained by thermal denaturation. It seems that many structural features of the native protein remain preserved under pressure denaturation. Experimental evidence comes from NMR experiments [6], but also from IR experiments [20, 21, 37, 38].

Figure 5.17 shows another experiment [56], namely a neutron-scattering experiment with myoglobin as a target from which the conservation of native structural elements in the denatured state is directly seen. Myoglobin denatures at pH 7 in the range between 0.3 and 0.4 GPa as judged from the optical absorption spectrum of the heme group. The corresponding changes in the protein structure and at the protein–water interface can be deduced from the neutron structure factor $H(Q)$ of a concentrated solution of myoglobin in D_2O (Figure 5.17). Q denotes the length of the scattering vector. The large maximum around $Q = 2\,\text{Å}^{-1}$ arises from O–O cor-

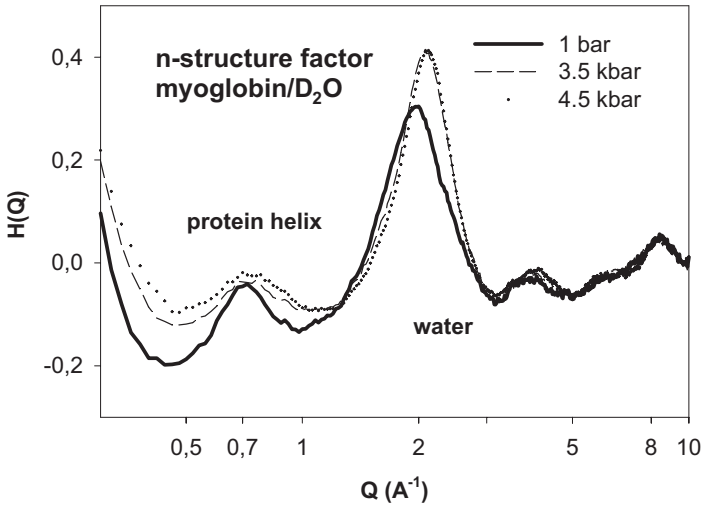

Fig. 5.17. Comparative neutron scattering experiments at ambient pressure and at high pressure. Plotted is the neutron structure factor $H(Q)$ as a function of Q. Data are for myoglobin. The important feature is the partial persistence of the protein helical structure (peak at $Q = 0.7\,\text{Å}^{-1}$) in the pressure-denatured state.

relations of water near the protein interface. This maximum increases with density. The smaller maximum near $Q = 0.7\,\text{Å}^{-1}$ reflects inter-helix correlations. The contrast is provided by the negative scattering length density of the protein hydrogen atoms versus the positive scattering length density of C, N, and O. The most remarkable feature is the persistence of this maximum above the transition at 0.45 GPa, indicating residual secondary structure in the pressure-unfolded form.

5.6 Conclusions and Outlook

Folding and denaturing processes of proteins are extremely complicated due to the complex nature of the protein molecules with their huge manifold of structural states. Hence, it is surprising that some of the characteristic features of equilibrium thermodynamics associated with the folded and denatured state are already revealed on the basis of simple models. Most important in this context is the reduction of the folding and denaturing processes to just two essential states, namely the native state and the denatured state. To reconcile this crude assumption with the large structural phase space, we introduced the concept of ''state lumping.'' Another important approximation concerns the vanishing higher (higher than two) derivatives of the chemical potential, rendering pressure- and temperature-independent state parameters (specific heat, compressibility, thermal expansion) to the protein. The result of these simplifying assumptions is an elliptically shaped

stability phase diagram, provided that the sign of the change in the specific heat capacity and in the compressibility is the same.

Our experiments on the stability of a modified cytochrome *c* in a glycerol/water solvent showed an almost perfect ellipse from which the regimes with positive and negative volume changes as well as positive and negative entropy changes could be deduced. We tried to shed some light on the microscopic aspects responsible for these regimes. A dominant force is the hydrophobic interaction which depends not only on temperature but also on pressure [57]. The characteristic structural features of the pressure-denatured state are different from the respective ones of the thermally denatured state. In both cases, however, water molecules come very close to the chromophore.

As to the open questions in context with the stability phase diagram, we refer to the elliptic shape. So far only closed diagrams have been observed, and in most cases an elliptic shape was an appropriate description. The question comes up how general this observation is and what the microscopic implications are. Admittedly, up to now few experiments have measured the full diagram.

Another problem concerns negative pressure. From an experimental point of view negative pressures as low as −200 bar seem to be feasible. Denaturation under negative pressure, that is under conditions where the relevant interactions are weakened, would add valuable information on pressure-induced denaturing forces.

Finally the role of the solvent has to be addressed in more detail. The solvent may have a dramatic influence on the hydrophobic interaction, the size of the solvent molecules may play an important role in all processes involving pressure, and, last but not least, understanding the influence of the solvent may also shed light on the behavior of membrane proteins.

Acknowledgment

The authors acknowledge financial support from the DFG (FOR 358, A1/2), from the Fonds der Chemischen Industrie (J.F.) and from the Bundesministerium für Bildung und Forschung 03DOE2M1.

Scientific input to this work came from many of our friends. We want to thank J. M. Vanderkooi, H. Lesch, and R. Gebhardt.

References

1 G. Weber, H. Drickammer, *Q. Rev. Biophys.* **1983**, *16*, 89–112.
2 Special Issue on ''Frontiers in high pressure biochemistry and biophysics'', *Biochim. Biophys. Acta* 2002, 1595, Issue 1–2.
3 C. A. Royer, *Biochim. Biophys. Acta* **2002**, *1595*, 201–209.
4 M. Gerstein, C. Gothia, *Proc. Natl Acad. Sci. USA* **1996**, *93*, 10167–10172.
5 A. Fersht, *Structure and Mechanism in Protein Science*, W. H. Freeman, New York, 1999.
6 D. P. Nash, J. Jonas, *Biochemistry* **1997**, *36*, 14375–14383.

7 G. J. A. Vidugiris, J. L. Markley, C. A. Royer, *Biochemistry* **1995**, *34*, 4909–4912.
8 P. L. Privalov, *Adv. Protein Chem.* **1979**, *33*, 167–241.
9 P. L. Privalov, S. J. Gill, *Adv. Protein Chem.* **1988**, *39*, 191–234.
10 G. I. Makhatadze, P. L. Privalov, *Adv. Protein Chem.* **1995**, *47*, 307–425.
11 J. F. Brandts, *J. Am. Chem. Soc.* **1964**, *86*, 4302–4314.
12 J. F. Brandts, *J. Am. Chem. Soc.* **1965**, *87*, 2759–2760.
13 A. Cooper, *Prog. Biophys. Mol. Biol.* **1984**, *44*, 181–214.
14 S. A. Hawley, *Biochemistry* **1971**, *10*, 2436–2442.
15 P. E. Cladis, R. K. Bogardus, W. B. Daniels, G. N. Taylor, *Phys. Rev. Lett.* **1977**, *39*, 720–723.
16 D. D. Klug, E. J. Whalley, *J. Chem. Phys.* **1979**, *71*, 1874–1877.
17 N. A. Clark, *J. Physique* **1979**, *40*, 345–349.
18 A. Zipp, W. Kauzmann, *Biochemistry* **1973**, *12*, 4217–4228.
19 H. Ludwig, W. Scigalla, B. Sojka, in *High Pressure Effects in Molecular Biophysics and Enzymology*, J. L. Markley, D. Northrop, C. A. Royer (Eds), Oxford University Press, Oxford, 1996, 346–363.
20 K. Heremans, L. Smeller, *Biochim. Biophys. Acta* **1998**, *1386*, 353–370.
21 Y. Taniguchi, N. Takeda, in *High Pressure Effects in Molecular Biophysics and Enzymology*, J. L. Markley, D. Northrop, C. A. Royer (Eds), Oxford University Press, Oxford, 1996, 87–95.
22 E. Paci, *Biochim. Biophys. Acta* **2002**, *1595*, 185–200.
23 R. Baldwin, *Proc. Natl Acad. Sci. USA* **1986**, *83*, 8069–8072.
24 R. Baldwin, N. Muller, *Proc. Natl Acad. Sci. USA* **1992**, *89*, 7110–7113.
25 P. L. Privalov, *Biofizika* **1987**, *32*, 742–746.
26 Y. V. Griko, P. Privalov, *J. Mol. Biol.* **1994**, *235*, 1318–1325.
27 Th. Kiefhaber, R. L. Baldwin, *J. Mol. Biol.* **1995**, *252*, 122–132.
28 M. Berthelot, *Ann. Chim.* **1850**, *30*, 232–237.
29 L. J. Briggs, *J. Appl. Phys.* **1950**, *21*, 721–722.
30 M. Eftink, G. Ramsey, in *High Pressure Effects in Molecular Biophysics and Enzymology*, J. Markley, D. Northrop, C. A. Royer (Eds), Oxford University Press, Oxford, 1996, 62.
31 T. V. Chalikian, K. J. Breslauer, *Curr. Opin. Struct. Biol.* **1998**, *8*, 657–664.
32 K. Gekko, H. Noguchi, *J. Phys. Chem.* **1979**, *83*, 2706–2714.
33 B. Gavish, E. Gratton, C. J. Hardy, *Proc. Natl Acad. Sci. USA* **1983**, *80*, 750–754.
34 J. Zollfrank, J. Friedrich, *J. Opt. Soc. Am. B.* **1992**, *9*, 956–961.
35 D. P. Kharakoz, A. P. Sarvazyan, *Biopolymers* **1993**, *33*, 11–25.
36 G. J. A. Vidugiris, C. A. Royer, *Biophys. J.* **1998**, *75*, 463–470.
37 G. Panick, R. Malessa, R. Winter, G. Rapp, K. J. Frye, C. A. Royer, *J. Mol. Biol.* **1998**, *275*, 389–402.
38 H. Herberhold, S. Marchal, R. Lange, C. H. Scheying, R. F. Vogel, R. Winter, *J. Mol. Biol.* **2003**, *330*, 1153–1164.
39 H. Lesch, H. Stadlbauer, J. Friedrich, J. M. Vanderkooi, *Biophys. J.* **2002**, *82*, 1644–1653.
40 M. Eremets, *High Pressure Experimental Methods*, Oxford University Press, Oxford, 1996.
41 J. D. Bryngelson, J. N. Onuchic, N. D. Socchi, P. G. Wolynes, *Proteins Struct. Funct. Genet.* **1995**, *21*, 167–195.
42 H. Frauenfelder, F. Parak, R. D. Young, in *Annu. Rev. Biophys. Chem.* **1988**, *17*, 451–479.
43 H. Frauenfelder, S. G. Sligar, P. G. Wolynes, *Science* **1991**, *254*, 1598–1603.
44 H. Frauenfelder, D. Thorn Leeson, *Nat. Struct. Biol.* **1998**, *5*, 757–759.
45 H. Frauenfelder, *Nat. Struct. Biol.* **1995**, *2*, 821–823.
46 A. E. Garcia, R. Blumenfeld, G. Hummer, J. A. Krummhansl, *Physica D* **1997**, *107*, 225–239.
47 K. A. Dill, H. S. Chan, *Nat. Struct. Biol.* **1997**, *4*, 10–19.
48 N. S. Bayliss, *J. Chem. Phys.* **1950**, *18*, 292–296.

49 N. S. Bayliss, E. G. McRae, *J. Phys. Chem.* **1954**, *58*, 1002–1006.

50 W. Liptay, *Z. Naturforsch.* **1965**, *20a*, 272–289.

51 W. Kauzmann, *Nature* **1987**, *325*, 763–764.

52 G. Hummer, S. Garde, A. E. Garcia, M. E. Paulalitis, L. R. Pratt, *Proc. Natl Acad. Sci. USA* **1998**, *95*, 1552–1555.

53 G. Hummer, S. Garde, A. E. Garcia, M. E. Paulalitis, L. R. Pratt, *J. Phys. Chem.* **1998**, *102*, 10469–10482.

54 A. C. Oliveira, L. P. Gaspart, A. T. Da Poian, J. L. Silva, *J. Mol. Biol.* **1994**, *240*, 184–187.

55 H. Lesch, J. Schlichter, J. Friedrich, J. M. Vanderkooi, *Biophys. J.* 2004, accepted.

56 W. Doster, R. Gebhardt, A. K. Soper, in *Advances in High Pressure Bioscience and Biotechnology*, R. Winter (Ed.), Springer, Berlin, 2003, 29.

57 K. A. Dill, *Biochemistry* **1990**, *29*, 7133–7155.